A Universal Route to Fabricate n-i-p Multi-Junction Polymer Solar Cells via Solution Processing

Peer-reviewed author version

Rasi, Dario Di Carlo; Hendriks, Koen H.; HEINTGES, Gael; Simone, Giulio; Gelinck, Gerwin H.; Gevaerts, Veronique S.; Andriessen, Ronn; PIROTTE, Geert; MAES, Wouter; Li, Weiwei; Wienk, Martijn M. & Janssen, Rene A. J. (2018) A Universal Route to Fabricate n-i-p Multi-Junction Polymer Solar Cells via Solution Processing.
In: SOLAR RRL, 2(5) (Art N° 1800018).

DOI: 10.1002/solr.201800018
Handle: http://hdl.handle.net/1942/27910

DOI: 10.1002/ ((please add manuscript number))
Article type: Full Paper

A universal route to fabricate *n-i-p* multi-junction polymer solar cells via solution processing

*Dario Di Carlo Rasi, Koen H. Hendriks, Gaël H. L. Heintges, Giulio Simone, Gerwin H. Gelinck, Veronique S. Gevaerts, Ronn Andriessen, Geert Pirotte, Wouter Maes, Weiwei Li, Martijn M. Wienk, and René A. J. Janssen**

D. Di Carlo Rasi, Dr. K. H. Hendriks, G. H. L. Heintges, G. Simone, Prof. G. H. Gelinck, Dr. M. M. Wienk, Prof. R. A. J. Janssen
Molecular Materials and Nanosystems & Institute for Complex Molecular Systems, Eindhoven University of Technology, P.O. Box 513, 5600 MB, Eindhoven, The Netherlands

G. Simone, Prof. G. H. Gelinck
Holst Centre, High Tech Campus 31, 5656 AE, Eindhoven, The Netherlands

Dr. V. S. Gevaerts
ECN – Solliance, High Tech Campus 21, 5656 AE, Eindhoven, The Netherlands

Dr. R. Andriessen
Holst Centre – Solliance, High Tech Campus 21, 5656 AE, Eindhoven, The Netherlands

G. H. L. Heintges, Dr. G. Pirotte, Prof. W. Maes
UHasselt – Hasselt University, Institute for Materials Research (IMO-IMOMEC), Design & Synthesis of Organic Semiconductors (DSOS), Agoralaan – Building D, 3590 Diepenbeek, Belgium

Prof. W. Li
Beijing National Laboratory for Molecular Sciences, CAS Key Laboratory of Organic Solids, Institute of Chemistry, Chinese Academy of Sciences, Beijing 100190, P. R. China

Dr. K. H. Hendriks, Dr. M. M. Wienk, Prof. R. A. J. Janssen
Dutch Institute for Fundamental Energy Research, De Zaale 20, 5612 AJ, Eindhoven, The Netherlands

Correspondence to: Prof. R. A. J. Janssen (E-mail: r.a.j.janssen@tue.nl)
Keywords: organic multi-junction solar cells, charge recombination layer, interconnection layer, inverted organic solar cells

Abstract

The interconnection layer (ICL) that connects adjacent subcells electrically and optically in solution-processed multi-junction polymer solar cells must meet functional requirements in terms of work functions, conductivity, and transparency, but also be compatible with the multiple layer stack in terms of processing and deposition conditions. Using a combination of poly(3,4-ethylenedioxythiophene):polystyrene sulfonate, diluted in near azeotropic water/*n*-propanol dispersions as hole transport layer, and ZnO nanoparticles, dispersed in isoamyl alcohol as electron transport layer, a novel, versatile ICL has been developed for solution-processed tandem and triple-junction solar cells in an *n-i-p* architecture. The ICL has been incorporated in six different tandem cells and three different triple-junction solar cells, employing a range of different polymer-fullerene photoactive layers. The new ICL provided an essentially lossless contact in each case, without the need of adjusting the formulations or deposition conditions. The approach permitted realizing complex devices in good yields, providing a power conversion efficiency up to 10%.

1. Introduction

Converting and storing energy from the sun represents one of the most important challenges for the sustainable development of anthropic activities. The traditional technology based on inorganic materials like silicon already provides very good performance. Pronounced interest arose in the recent years in solar cells based on organic materials, which can be processed not only by vacuum techniques but also from solution.[1-3] This paves the way towards competitive energy pay-back time as well as attractive niche applications in which the device can be bended, stretched, folded, color-tuned and can be semitransparent.[4-8] The most successful concept for the realization of organic solar cells is the so-called bulk heterojunction: an intimate mix of electron donating and electron accepting materials with domain sizes on the nanometer scale. By carefully engineering the chemical structure of the organic semiconductors, their optical, electronic, and morphological properties can be conveniently tuned to improve the performance. Efficiencies of solution-processed organic solar cells have seen a tremendous increase, reaching 13% power conversion efficiency recently.[9] Aiming at even further improving this performance, the concept of multi-junction solar cells has been introduced and optimized into the organic framework and an efficiency above 13% has been reported for tandem solar cells processed entirely from solution, apart from the bottom and top electrodes.[10] The most efficient organic tandem solar cells involve series-connected subcells with photoactive layers of complementary band gaps (E_g) and it is this architecture that we are considering in this study. The voltages provided by the different subcells are added up, at the expense of the current, which is limited by the subcell generating the least charges. By carefully choosing active layers with complementary absorption, the loss in current can be overcompensated by the gain in voltage, resulting in a higher efficiency.

The main challenge in developing a procedure for making multi-junction solar cells from solution is the fabrication of the interconnecting layer (ICL). The ICL is composed of charge-selective interlayer materials that ensure the recombination of opposite charges from two adjacent active layers, without energy loss. This is done by stacking an electron transport material and a hole transport material. Efficient, solution-processable ICLs should satisfy a number of requirements:

(1) The Fermi levels of the ICL must match with the relevant highest occupied molecular orbital (HOMO) and lowest unoccupied molecular orbital LUMO energy levels of the organic materials in the adjacent active layers that are sandwiching the ICL to create Ohmic contacts.

(2) The materials in the ICL should possess sufficient Ohmic conductance to enable fast recombination of charges and to avoid loss of potential energy or fill factor.
(3) The parasitic absorption of sunlight should be low.
(4) The temperatures at which the processing and any post-treatment are performed should not deteriorate the performance of the active layers in the device.
(5) The formulation of the solutions from which the ICL is cast should not interfere with the underlying materials in the sequence of the device stack.
(6) The ICL should prevent that the solvents that are used to deposit subsequent layers in the stack, penetrate and dissolve underlying layers.
(7) The processing of the ICL should be versatile, so that it can be used for many combinations of active layers from different materials.

In recent years, several different combinations of materials have been proposed as ICL, involving either organic materials or transparent semiconducting metal oxides.[10-24] For the selective extraction of holes from the photoactive layers poly(3,4-ethylenedioxythiophene):polystyrene sulfonate (PEDOT:PSS) is widely used but also metal oxides such as MoO_3,[25] V_2O_5,[26] and WO_3,[27] or graphene oxide (GO)[28] can be used for the purpose. For selective electron extraction, solution-processed metal oxides such as ZnO nanoparticles,[29] sol-gel TiO_x,[11] or Li-doped ZnO[30] are popular. These metal oxides can be covered by self-assembled monolayers [31] or poly[(9,9-bis(3'-(*N*,*N*-dimethylamion)propyl)-2,7-fluorene)-*alt*-2,7-(9,9-dioctyl)-fluorene] (PFN)[32] to improve charge selectivity. Also polyamines such ethoxylated polyethylenimine (PEIE)[33] and polyethylenimine (PEI)[34] have been used to modify the work function of PEDOT:PSS or metal oxides to create an effective low work function, electron selective contact. One of the reasons for the large variety of ICLs stems from the fact that the proposed materials or their processing conditions are often quite specific to the nature of the photoactive layers. A universal, solution-based method that works in combination with a large number of different active layers does not exist at present. The choice of ICL and the details of its casting conditions (mainly the formulation of the solutions) do vary substantially according to the particular stack of materials under consideration, to ensure the so-called orthogonality of casting solvents (related to requirements (5) and (6) above). The match of the surface energy of the inks from which we process the ICL to the surface energy of the organic active layer plays a major role in the formation of the film.[35] Regarding requirement (4), we note that for some of the materials used in this work even mild

temperatures like 60 °C decrease the photovoltaic performance of the photoactive layer, probably due to morphology changes. Hence, a universal route to fabricate multi-junction polymer solar cells via solution processing at mild temperatures is in great demand.

Herein, we describe a combination of interlayers and processing conditions that fulfill the entire list of requirements. We developed new formulations for dispersions of PEDOT:PSS and ZnO nanoparticles in solvents that enable orthogonal processing of the ICL on any photoactive layer in an inverted (*n-i-p*) configuration we have tested. The reasons to choose for PEDOT:PSS and ZnO are their favorable work functions, and room temperature deposition conditions from benign solvents. To demonstrate this, we combined photoactive layers based on polymer-fullerene blends of different nature to fabricate six tandem and three triple-junction solar cells. A total of eight different active layers were tested in varying configurations, as front or back subcells in tandems, or as a middle subcell in triple-junctions. The performance characteristics of these multi-junction devices were, in general, in good agreement with the expected performance based on the properties of corresponding single-junction devices. As proof of concept, triple-junction solar cells with a power conversion efficiency of 10% were realized with excellent statistical relevance (yield 94%).

2. Results and Discussion

2.1. Materials and device architectures

To develop a versatile method for coating the ICL in different device stacks we decided to develop and test ICL formulations on active layer materials of different chemical nature and with different opto-electrical properties, suitable for different roles in tandem and triple-junction cells. We adopted an inverted (*n-i-p*) device configuration in which the electron transporting layer (ETL) is deposited first, followed by the active layer and the hole transport layer (HTL). There are several reasons to prefer an inverted (*n-i-p*) over a conventional (*p-i-n*) device architecture, mainly related to the use of PEDOT:PSS as HTL. In the conventional structure, the HTL is positioned between the light source and the photoactive layer, which leads to parasitic absorption by the polaron/bipolaron absorption bands of PEDOT:PSS in the near infrared.[36] Further, the acidic nature of the commercial PEDOT:PSS dispersions in water causes that it cannot be deposited on ZnO without deteriorating this layer or even washing it away completely. Increasing the pH of the dispersion can mitigate this, but lowers the work function of the resulting PEDOT:PSS layer. In turn this limits the open-circuit voltage (V_{OC}) that can be reached and necessitates the use of additional MoO_x or Nafion layers to compensate

for this loss.[37] Reversing the processing order of the ZnO and PEDOT:PSS layers avoids these complications. Finally, the Ag back electrode that is commonly used in the *n-i-p* configuration is more reflective than the Al back contact in most *p-i-n* structures.[38] The general sequence of layers in single, double and triple-junction devices used in this work is shown in **Figure 1**.

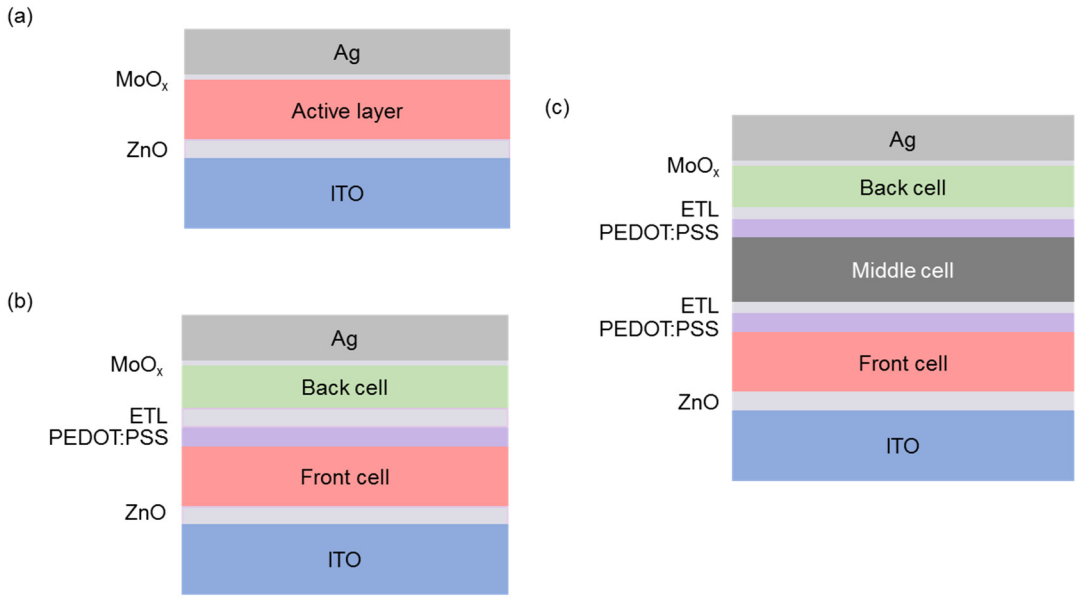

Figure 1. Device architecture of *n-i-p* (a) single, (b), double, and (c) triple-junction solar cells adopted in this work.

The optimal position of an organic semiconductor layer in a multi-junction stack is dictated by its optical band gap: wide band gap materials are preferably close to the transparent electrode (front subcell), while low band gap materials are close to the reflecting back contact (back subcell). This generally represents an optimal choice because the high energy of photons from the blue part of the solar spectrum would be lost by thermalization if these were absorbed by the low band gap material. Materials with an intermediate band gap can be conveniently used in various positions, especially as middle cell in triple-junction solar cells.

Figure 2 shows the donor polymers tested in this study. We used PCDTBT (E_g = 1.88 eV), PBDTTPD (E_g = 1.85 eV), and PDCBT (E_g = 1.90 eV) as wide band gap donors in the front subcells.[39,40,41] For the back subcells we selected PDPP5T (E_g = 1.46 eV), PDPP3T (E_g = 1.33 eV), and its methylated version PMDPP3T (E_g = 1.30 eV) as donors.[13,42,43] Donors that were used either in the front, middle, or back subcells were PDPPTPT (E_g = 1.53 eV) and

PTB7-Th (E_g = 1.58 eV).[44,45] All donors were used in combination with [6,6]-phenyl-C_{61}-butyric acid methyl ester ($PC_{60}BM$) or [6,6]-phenyl-C_{71}-butyric acid methyl ester ($PC_{70}BM$).

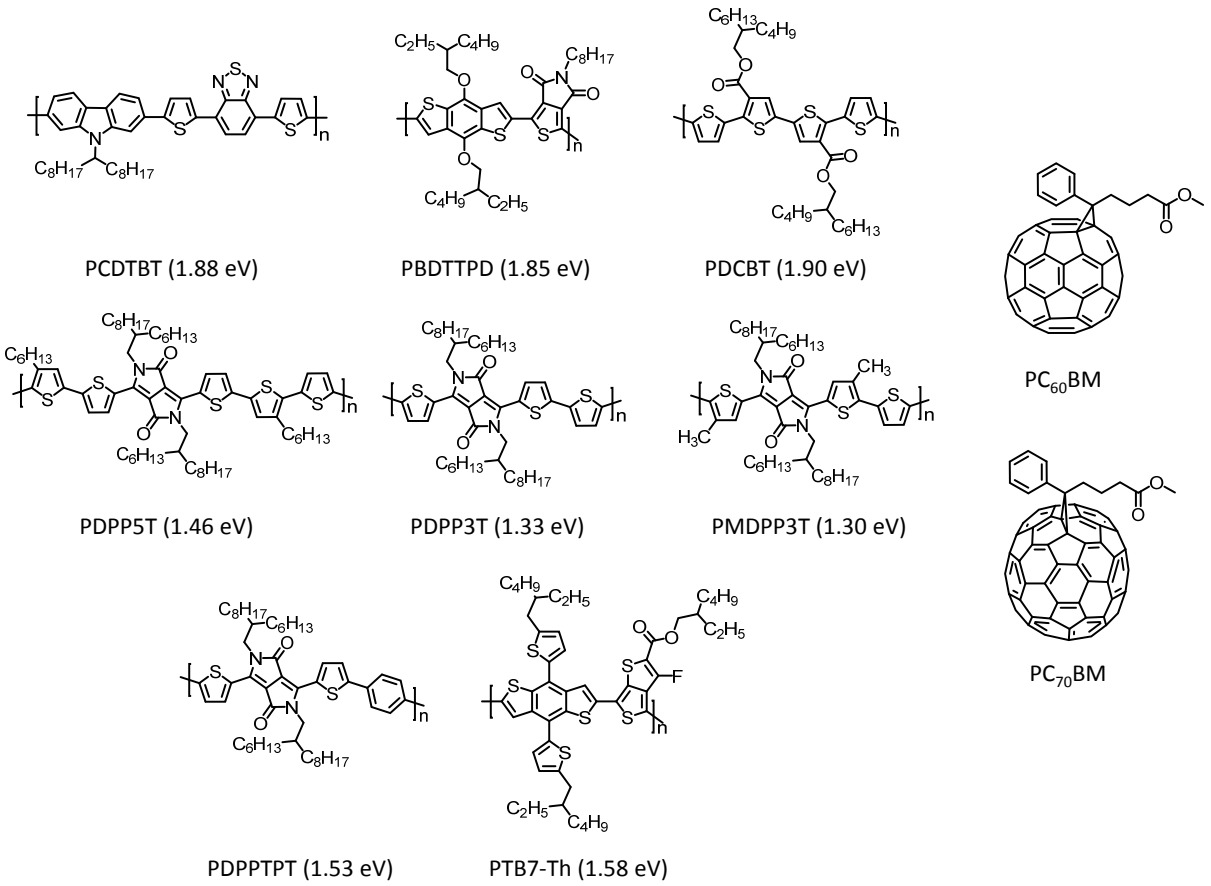

Figure 2. Chemical structures of the donor polymers and fullerene derivative acceptors used in this study. The corresponding optical band gaps are shown in parenthesis. Systematic names of the polymers are collected in Table S1 (Supporting Information).

Table 1 lists the optimized photovoltaic performance under simulated air mass 1.5 (AM1.5G) solar radiation of each of the eight donor polymers in combination with either $PC_{60}BM$ or $PC_{70}BM$ as acceptor in an *n-i-p* device configuration using sol-gel ZnO as ETL and MoO_x as HTL with indium tin oxide (ITO) and silver as electrodes. We labelled each blend as BHJ*n*, *n* being a number for further reference. Details on the processing conditions for each cell can be found in the Experimental Section.

Table 1. Photovoltaic performance of the inverted single-junction solar cells with optimized thickness.

	Blend	V_{OC} [V]	J_{SC} [mA cm^{-2}]	FF	PCE [%]
BHJ1	PCDTBT:$PC_{70}BM$	0.88	9.04	0.63	5.0
BHJ2	PBDTTPD:$PC_{70}BM$	0.90	11.9	0.66	7.1
BHJ3	PDCBT:$PC_{60}BM$	0.86	8.73	0.71	5.3
BHJ4	PDPPTPT:$PC_{60}BM$	0.79	12.1	0.64	6.3
BHJ5	PTB7-Th:$PC_{70}BM$	0.79	16.9	0.69	9.2
BHJ6	PDPP5T:$PC_{60}BM$	0.57	14.6	0.65	5.4
BHJ7	PDPP3T:$PC_{60}BM$	0.68	11.8	0.68	5.4
BHJ8	PMDPP3T:$PC_{60}BM$	0.61	15.6	0.63	5.7

2.2. PEDOT:PSS as HTL

PEDOT:PSS is used in many organic solar cells as HTL. PEDOT:PSS is generally deposited from a dispersion in water at low pH. In principle the use of water is advantageous because it is an orthogonal solvent to the organic photoactive layers. On the other hand, the surface energy of water (72.8 mN m^{-1}) is so high that the PEDOT:PSS dispersion poorly wets the surface of organic semiconductors and mostly flies off during the spin-coating. Different modifications of commercial PEDOT:PSS dispersions have been proposed to improve the deposition of PEDOT:PSS on top of a photoactive layer, while preserving the functional properties. Examples are the use of isopropanol[31,34,46,47] or surfactants[48-53] to change the wettability, or sodium polystyrene sulfonate (SPS) to change the viscosity.[35] Modifications that involve solid and liquid additives can also alter properties of PEDOT:PSS like the conductivity and the work function.

In this work, we introduce a novel formulation of PEDOT:PSS based on adding *n*-propanol. We found that dropwise addition of *n*-propanol to the commercial PEDOT:PSS (Clevios P VPAl 4083) dispersion in water over 15 minutes under vigorous stirring results in a stable dispersion. *n*-Propanol has a much lower surface energy (23.7 mN m^{-1}), which improves the wetting of the diluted dispersion on organic surfaces. Furthermore the 1:2 volume ratio of water to *n*-propanol (0.38:0.62 w/w) is fairly close to the azeotropic composition (0.28:0.72 w/w). This ensures that during evaporation the evaporating layer will contain an appreciable amount of *n*-propanol, such that de-wetting during drying is prevented.[54] The use of *n*-propanol has a distinct advantage over the use of isopropanol. The water-isopropanol azeotrope (0.12:0.88 w/w) is much richer in the alcohol, implying that more isopropanol than

n-propanol must be added to the aqueous PEDOT:PSS dispersion to reach (near) azeotropic evaporation. This results in PEDOT:PSS thinner layers. In the following we refer to this new formulation as D-PEDOT:PSS (diluted in *n*-propanol). We remark that *n*-propanol evaporates virtually completely during spin-coating, leaving nothing more than just PEDOT:PSS in the layer.

We optimized the amount of *n*-propanol that is necessary to uniformly cover the active layer. **Figure 3** shows pictures taken with a camera of three different bulk heterojunction layers, before and after spin-coating of D-PEDOT:PSS on top. For the deposition we used spin-coating at 500 rpm in a nitrogen filled glove box, which was found to improve the wetting. Figure 3 shows that dilution of PEDOT:PSS with *n*-propanol improved the film formation properties. On a PCDTBT:$PC_{70}BM$ layer, a ratio of water/*n*-propanol 1:1 (v/v) seemed sufficient to form a uniform film of PEDOT:PSS on top. For PDPPTPT:$PC_{60}BM$ and PDPP5T:$PC_{60}BM$, however, the PEDOT:PSS 1:1 (v/v) diluted dispersion in water/*n*-propanol only partially covered the surface, possibly due to a larger difference in surface energy of these substrates. By further diluting to 1:2 (v/v), the coverage turned uniform for each of the cases considered. The same 1:2 (v/v) formulation turned out to deposit well on many other active layers. As explained, the 1:2 mixture corresponds to a mass fraction of *n*-propanol of 0.62, close to the azeotropic composition of 0.72. Hence in the last stages of the drying process, mostly water is present in the layer, which is the native medium of PEDOT:PSS, but the viscosity at this point has increased because of the increased PEDOT:PSS concentration such that dewetting or material flying off from the substrate does not occur. After spin-coating the D-PEDOT:PSS layers were kept in a vacuum of $\sim 10^{-2}$ mbar for 30 minutes to remove residual solvents, and no further treatment was performed.

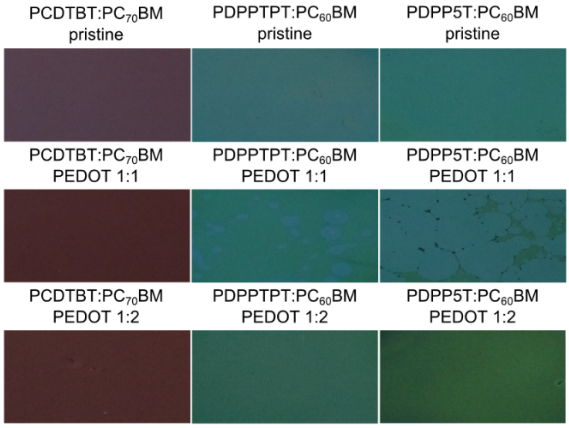

Figure 3. Photographs of glass substrates coated with different bulk heterojunction layers without and with an additional layer of PEDOT:PSS processed from water/*n*-propanol mixtures with different volume ratios.

To optimize the performance of D-PEDOT:PSS as HTL, we made single-junction solar cells based on BHJ1 with a ITO/PEIE/BHJ1/D-PEDOT:PSS/Ag architecture, using PEIE as an ETL.[55] Different dilutions with *n*-propanol were compared and the photovoltaic parameters determined under simulated solar illumination are collected in **Table 2** and compared to a reference cell in which D-PEDOT:PSS was replaced by a layer of MoO_x. Dilution with *n*-propanol reduces the thickness of the D-PEDOT:PSS films. Table 2 reveals that the amount of *n*-propanol mainly affected the short-circuit current density (J_{SC}) and the fill factor (FF). Starting from 1:2 dilution, the power conversion efficiency (PCE) remains constant. The difference in J_{SC} with respect to the reference device is related to optical cavity effects as inferred from optical modelling. Apart from this, only minor differences in the FF occurred. Table 2 shows that going beyond 1:2 of dilution brings no improvement. Therefore, we adopted the 1:2 (v/v) water/*n*-propanol ratio as the standard for D-PEDOT:PSS.

Table 2. Photovoltaic parameters of ITO/PEIE/PCDTBT:$PC_{70}BM$/D-PEDOT:PSS/Ag solar cells with a PEDOT:PSS layer processed from different water/*n*-propanol (v/v) dispersions.

PEDOT:PSS:*n*-propanol	V_{OC} [V]	J_{SC} [mA cm^{-2}]	FF	PCE [%]
Reference [a)]	0.87	8.2	0.56	4.0
1:1 (70 nm)	0.86	6.1	0.61	3.2
1:2 (40 nm)	0.89	7.2	0.61	3.9
1:3 (30 nm)	0.88	7.8	0.57	3.9
1:4 (25 nm)	0.87	7.8	0.58	3.9
1:5 (20 nm)	0.88	7.8	0.57	3.8

[a)] ITO/PEIE/PCDTBT:$PC_{70}BM$/MoO_x/Ag.

2.3. PEIE and ZnO nanoparticles as ETL

To create an ICL for tandem solar cells the optimized D-PEDOT:PSS layer must be combined with an ETL (Figure 1). We decided to test both PEIE and ZnO nanoparticles on top of the D-PEDOT:PSS film. The function of PEIE is to create a thin (< 10 nm) layer in which the presence of dipoles or ions at the interface lowers the work function of PEDOT:PSS, permitting the tunneling of electrons.[55] PEIE is commercially available as an aqueous solution, but water is not a suitable solvent for processing on top of PEDOT:PSS layers. Following the procedure of Lee *et al.* [34] for the non-ethoxylated version of polyethylenimine (PEI), we diluted PEIE with a significant amount of isopropanol (IPA) to reach concentrations in IPA around 0.2 wt%. By doing so the content in water reduced to a marginal amount (in the same order of magnitude as PEIE), avoiding the dissolution of the PEDOT:PSS layer. PEIE is an insulating material and therefore an optimal coverage of the substrates is required in order to have correctly working devices. **Figure 4** shows how the *J-V* characteristics of ITO/D-PEDOT:PSS/PEIE/BHJ7/MoO_x/Ag single-junction devices change in relation to the concentration of PEIE in IPA. If the concentration is too low, the layer is too thin and, eventually, discontinuous, leading to a reduced FF. On the opposite, a too high concentration yields a too thick layer, which hinders tunneling of electrons and creates a barrier at this interface resulting in a lower J_{sc} and FF. At 0.2 wt% PEIE in IPA the device performance of the ITO/D-PEDOT:PSS/PEIE/BHJ7/MoO_x/Ag cells is very similar to that of the reference ITO/ZnO/BHJ7/MoO_x/Ag cell (Figure 4).

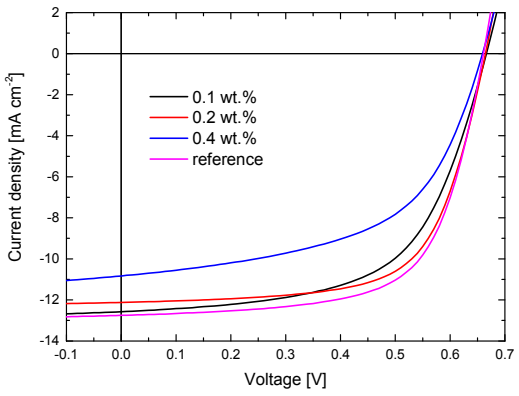

Figure 4. *J-V* characteristics of ITO/D-PEDOT:PSS/PEIE/BHJ7/MoO_x/Ag fabricated using different concentrations of PEIE in IPA in wt.%. The reference device with sol-gel ZnO on ITO instead of D-PEDOT:PSS/PEIE is shown for a comparison.

The ZnO nanoparticles were synthesized according to the procedure described in detail in the Supporting Information and were re-dispersed in isoamyl alcohol. Spin-coating the ZnO nanoparticles from isoamyl alcohol on top of a PEDOT:PSS layer is straightforward.

2.4. Tandems solar cells

The combination of D-PEDOT:PSS and PEIE or ZnO was used to realize a series of tandem solar cells featuring different active layer materials (**Table 3**). Given the complexity of a full thickness optimization of all layers, we used the optimum thickness of the photoactive layers of the single-junction cells. By doing so it was still possible to evaluate the quality of the ICL by checking the addition of the V_{OC}'s of the subcells. Also the FF of the tandem is determined by the *J-V* characteristics of both the subcells, and can be found from the mathematical sum of the *J-V* curves along the voltage axis, i.e. at constant current density. In practice the FF of the tandem cell is comparable to that of the current-limiting subcell. If the processing of the complete stack would degrade any of the layers, it would unavoidably lower the FF of the tandem cell.

Table 3. Photovoltaic performance of ITO/ZnO/BHJ/D-PEDOT:PSS/ETL/BHJ/MoO_x/Ag tandem solar cells with different active layer materials.

Tandem (Front-Back)	ETL	V_{OC} [a] [V]	V_{OC}^{sum} [b] [V]	J_{SC} [a] [mA cm^{-2}]	FF [a]	PCE [a] [%]	Yield
BHJ1-BHJ6	PEIE	1.47 (1.47)	1.45	6.3 (6.22)	0.62 (0.60)	5.7 (5.48)	4/4
BHJ2-BHJ4	PEIE	1.66 (1.66)	1.69	7.1 (7.04)	0.61 (0.60)	7.2 (7.05)	3/4
BHJ4-BHJ6	PEIE	1.33 (1.33)	1.36	6.9 (6.38)	0.63 (0.62)	5.7 (5.19)	7/8
BHJ7-BHJ7	PEIE	1.32 (1.30)	1.36	6.0 (5.98)	0.77 (0.70)	6.1 (5.46)	16/16
BHJ1-BHJ4 [c]	ZnO	1.68 (1.68)	1.67	7.1 (6.58)	0.62 (0.62)	7.3 (6.75)	6/8
BHJ4-BHJ6	ZnO	1.34 (1.34)	1.36	5.8 (5.36)	0.64 (0.61)	5.0 (4.36)	8/8
BHJ3-BHJ4	ZnO	1.54 (1.54)	1.65	6.8 (6.70)	0.66 (0.61)	6.9 (6.25)	3/4
BHJ4-BHJ8	ZnO	1.36 (1.37)	1.40	6.8 (6.81)	0.59 (0.55)	5.5 (5.10)	4/4
BHJ3-BHJ5	ZnO	1.57 (1.58)	1.65	7.8 (7.63)	0.61 (0.60)	7.4 (7.17)	4/4
BHJ5-BHJ8 [d]	ZnO	1.39 (1.39)	1.40	10.1 (9.98)	0.62 (0.62)	8.7 (8.61)	8/8

[a] Values in parenthesis are average values over the number of working devices tested.
[b] Sum of V_{OC}'s of the corresponding single-junction cells (Table 2).
[c] ITO/ZnO/BHJ1/D-PEDOT:PSS/ZnO/BHJ4/D-PEDOT:PSS/MoO_x/Ag.
[d] ITO/D-PEDOT:PSS/ZnO/BHJ5/D-PEDOT:PSS/ZnO/BHJ8/MoO_x/Ag.

The experimental V_{OC}'s generally agree within a few tens of mV with the value calculated from the sum of the corresponding single-junction devices (V_{OC}^{sum}). Only for the two tandem

cells featuring BHJ3 (PDCBT:$PC_{60}BM$) in the front cell a substantial loss in V_{OC} was found. In general a 10 to 20 mV loss can be expected because the effective light intensity in each of the subcells of a tandem is less than in a single-junction cell under AM1.5G illumination. This expected loss can be estimated using $\Delta V_{OC} = (kT/q)\ln[J_{SC}(\text{tandem})/J_{SC}(\text{single})]$, when the ideality factor of diode is unity.

For BHJ3, the loss is evidently much larger (up to 110 mV). We found that in a single-junction BHJ3 device, the V_{OC} is reduced by about 30 mV when a D-PEDOT:PSS/MoO_x/Ag top contact is used instead of MoO_x/Ag. Apparently the V_{OC} of BHJ3 is sensitive to the details of the processing or the nature of the top contact. Further evidence of the sensitivity of the V_{OC} of BHJ3 is shown in Figure S1 (Supporting Information) which compares the *J-V* characteristics of single-junction devices with thermal annealing either before or after evaporating the MoO_x/Ag top contact. The difference in V_{OC} is 100 mV. Presently, we cannot offer a consistent explanation for this difference, but apparently subtle changes in interface morphology or composition of BHJ3 in the two annealing procedures have a large effect on V_{OC}.

The quality of the tandem solar cells can also be evaluated by considering the FF. In a multi-junction device, the FF is influenced by the FF of each subcell, in particular by the subcell that limits the photocurrent. Comparing Table 1 and Table 3, we can see that the FF of the tandems BHJ1-BHJ6, BHJ4-BHJ6 (both with PEIE and ZnO), BHJ1-BHJ4, BHJ3-BHJ4 and BHJ5-BHJ8 is comparable ($\leq \pm 0.01$) with at least one of the corresponding single-junction cells. For BHJ2-BHJ4, BHJ4-BHJ8 and BHJ3-BHJ5 the corresponding loss in FF is larger, but the FF never went below 0.59. A special case is the BHJ7-BHJ7 tandem cell where the FF (0.77) was significantly higher than for the single-junction cell (0.68). A possible cause is the reduced light intensity experienced by each subcell (*e.g.* lower bimolecular recombination).

Measuring the external quantum efficiency (EQE) spectrum of a tandem cell gives insight in the current generated by each subcell, but also in the structural integrity of the layers, especially on the presence of current leakage paths in one or more photoactive layers. In an ideal tandem cell, the EQE measured without bias light should follow the lower envelope of the EQEs of the subcells, determined using representative bias light.[56] In case of a leakage, the EQE without bias light can be substantially higher.[56] **Figure 5** shows that the EQEs of BHJ2-BHJ4 (best tandem with PEIE as ETL) and BHJ5-BHJ8 (best tandem with ZnO as ETL) measured without light bias are very close to the expected behavior.

By comparison of V_{OC} and FF values and measuring EQE, we conclude that the D-PEDOT:PSS/PEIE and D-PEDOT:PSS/ZnO ICLs are suitable for use in a range of tandem cell configurations.

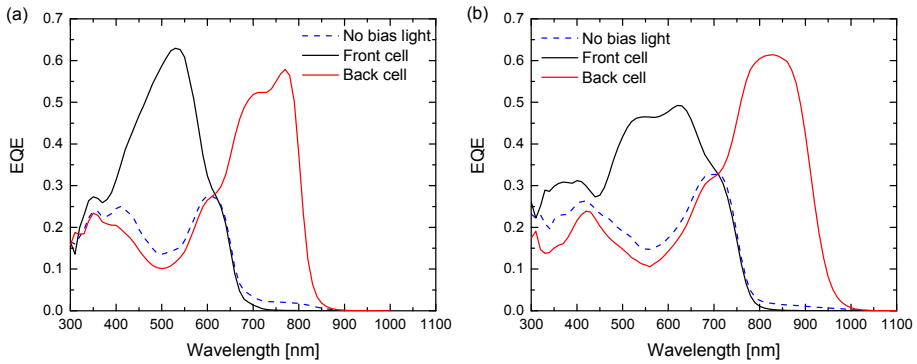

Figure 5. EQE spectra of BHJ2-BHJ4 (PEIE as ETL) and BHJ5-BHJ8 (ZnO as ETL) recorded with (solid lines) and without (dashed lines) bias light; for the nomenclature refer to Table 1. LED sources (530 and 730 nm (a) or 530 and 940 nm (b)) were used to optically bias the front and back subcells, respectively.

2.5. ICL for triple-junction solar cells: need for second order orthogonality

After demonstrating tandem solar cells using D-PEDOT:PSS/PEIE and D-PEDOT:PSS/ZnO as ICL, we studied the application of the same layers to fabricate triple-junction cells. To make triple junction cells, the ICL must withstand the deposition of a BHJ as well as a subsequent ICL. To test the compatibility of the layers with the solvents necessary for processing, we made ITO/D-PEDOT:PSS/PEIE/BHJ4/MoO_x/Ag single-junction cells and compared their performance with and without rinsing the BHJ4 layer with water/*n*-propanol (1:2), before evaporating the top contact. BHJ4 (PDPPTPT:$PC_{60}BM$) represents an attractive option as middle cell active layer. **Figure 6**a demonstrates that the water/*n*-propanol (1:2 v/v) mixture has a detrimental effect on the device performance. We observed similar behavior also with BHJ1 and BHJ6 as photoactive layer (see Figure S2 in the Supporting Information), implying that the effect is not related to the specific choice of the photoactive layer. To better understand the problem, we performed a similar experiment in which we used a ITO/D-PEDOT:PSS/ZnO/BHJ4/(D-PEDOT:PSS)/MoO_x/Ag cell, with and without the second layer of D-PEDOT:PSS on top of the active layer. Figure 6b shows that with ZnO on top of D-PEDOT:PSS the problem does not occur. We thus see that that the water/*n*-propanol (1:2 v/v) mixture disrupts the interface between PEDOT:PSS and PEIE, beneath the BHJ layer on which

the water/*n*-propanol mixture is processed. Fortuitously, this problem does not occur between D-PEDOT:PSS and the ZnO nanoparticles, such that a D-PEDOT:PSS layer can be processed on a D-PEDOT:PSS/ZnO/BHJ stack. This is remarkable because ZnO is sensitive to the acidic nature of the D-PEDOT:PSS dispersion and we speculate that acidic water does not penetrate the BHJ layer but *n*-propanol does. Given the suitability of the ZnO nanoparticle layer, we adopted this option instead of PEIE to fabricate triple-junction solar cells.

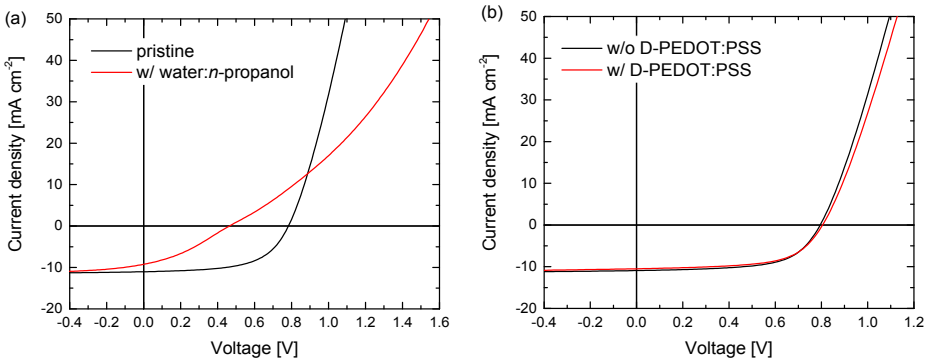

Figure 6. (a) *J-V* characteristics of an ITO/D-PEDOT:PSS/PEIE/BHJ4/MoO_x/Ag cell with and without rinsing the active layer with water/*n*-propanol (1:2) before evaporating the top contact. (b) *J-V* characteristics of an ITO/D-PEDOT:PSS/ZnO/BHJ4/(D-PEDOT:PSS)/MoO_x/Ag cell with and without the second layer of D-PEDOT:PSS on top of the active layer.

2.6. Triple-junction solar cells

We used D-PEDOT:PSS and ZnO nanoparticles to fabricate the ICLs of *n-i-p* triple-junction polymer solar cells (Figure 1) and first used BHJ1, BHJ4, and BHJ6 in the front, middle, and back subcells, respectively (**Table 4**) using the optimal thicknesses of the single-junction cell for each layer.

Table 4. Photovoltaic performance of ITO/ZnO/BHJ/D-PEDOT:PSS/ZnO/BHJ/D-PEDOT:PSS/ZnO/BHJ/MoO_x/Ag triple-junction solar cells with different active layer materials.

Triple (Front-Middle-Back)	V_{OC} [a] [V]	V_{OC}^{sum} [b] [V]	J_{SC} [a] [mA cm^{-2}]	FF [a]	PCE [a] [%]	Yield
BHJ1-BHJ4-BHJ6	2.26 (2.24)	2.24	4.4 (3.41)	0.61 (0.64)	6.0 (4.89)	12/12
BHJ3-BHJ4-BHJ8	2.20 (2.19)	2.26	6.0 (5.77)	0.66 (0.60)	8.7 (7.57)	12/12
BHJ3-BHJ5-BHJ8	2.15 (2.15)	2.26	6.9 (6.58)	0.68 (0.69)	10.0 (9.77)	15/16

[a] Values in parenthesis are average values over the number of working devices tested.
[b] Sum of V_{OC}'s of corresponding single-junction cells (Table 2).

By adding the values of V_{OC}'s of the single-junction cells from Table 1, a perfect match with the experimental value for the triple cells was found. Also the average FF is consistent with the FFs of the reference cells. The triple cells were fabricated with an excellent yield of 12 good devices out of 12 fabricated. Both the choice of the materials and the optical interference effects dramatically limited the best PCE (about 6%).

To improve the performance, we applied improved materials in the front (BHJ3) and back (BHJ8) subcells. The use of $PC_{60}BM$ in BHJ3 and BHJ8 of the front and back cells was aimed at sacrificing some of the light absorbed by the front and back cell in favor of the middle cell, which is usually current limiting. We further optimized the thickness of the active layers *via* semi-empirical opto-electrical modeling.[57] The procedure consists of three steps. First we determined the wavelength-dependent refractive index (n) and extinction coefficient (k) of each layer and determined the maximum current generated in single-junction cells using transfer matrix (TM) optical modelling and the AM1.5G spectrum. Next, we fabricated single-junction cells using a range of different active layer thicknesses and measured the *J-V* characteristics and the EQE. The internal quantum efficiency (IQE) of the single-junction at each thickness was determined as the ratio between the J_{SC} obtained by integrating the EQE with the AM1.5G spectrum and the maximum predicted J_{SC} according to the optical modeling. Finally, we scaled the experimental *J-V* characteristics of single-junction cells by the modeled, IQE-corrected J_{SC} value of each subcell and we combined these according to Kirchhoff's law to give the expected *J-V* characteristics of the triple-junction cell.[58] The last step is re-iterated for all thickness combinations of interest. All the relevant data are shown in Table S2 and Figure S3 (Supporting Information) or are available in the literature.[59] In the optimization, the thickness of the D-PEDOT:PSS (30 nm) and ZnO (20 nm) in the interconnection layer was kept constant. The results of the optimization are summarized in **Figure 7**.

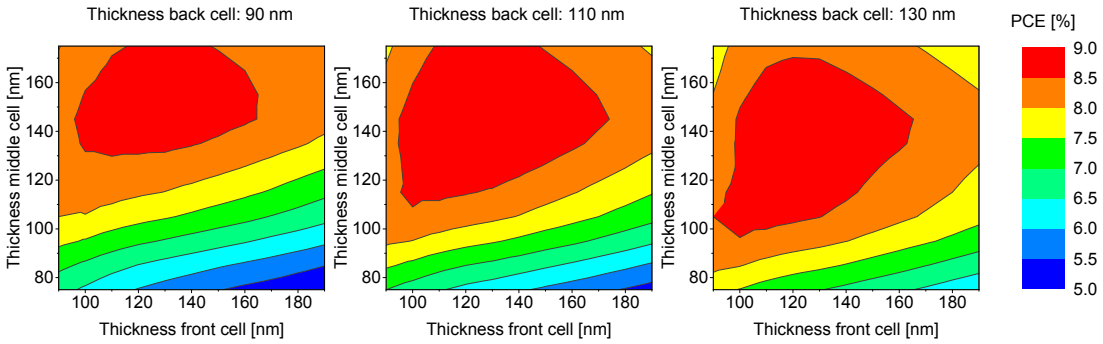

Figure 7. Expected PCE for an ITO/ZnO/BHJ3/D-PEDOT:PSS/ZnO/BHJ4/D-PEDOT:PSS/ZnO/BHJ8/MoO_x/Ag triple-junction solar cell as a function of the thickness of each active layer, according to opto-electrical modeling optimization.

On the basis of the modeling, we selected 130, 145, and 110 nm, respectively, for the front, middle, and back subcells. By using this combination of thicknesses, a PCE of around 9% was expected. Table 4 reveals that the PCE (8.7%) of the best cell is close to the predicted PCE. The difference is acceptable, considering the approximations adopted in the optimization. Similarly to the tandems with BHJ3, a 60 mV loss in the V_{OC} appeared also in this triple. The best FF (0.66) nicely lies in the middle of the range reported for the references.

The EQE of the triple junction cell was measured using appropriate light bias, voltage bias and light intensity corrections following the protocol described in detail recently.[59] From the EQE spectra in **Figure 8**a, it can be seen that the BHJ4 middle cell (PDPPTPT:$PC_{60}BM$) gave a low EQE signal, limiting the total current extracted from the device. Integration of the three EQEs with the AM1.5G spectrum gave 7.13, 5.70 and 6.63 mA cm^{-2}. The low current generated by the middle cell is due to the modest IQE = 0.64 at the optimal thickness (145 nm).

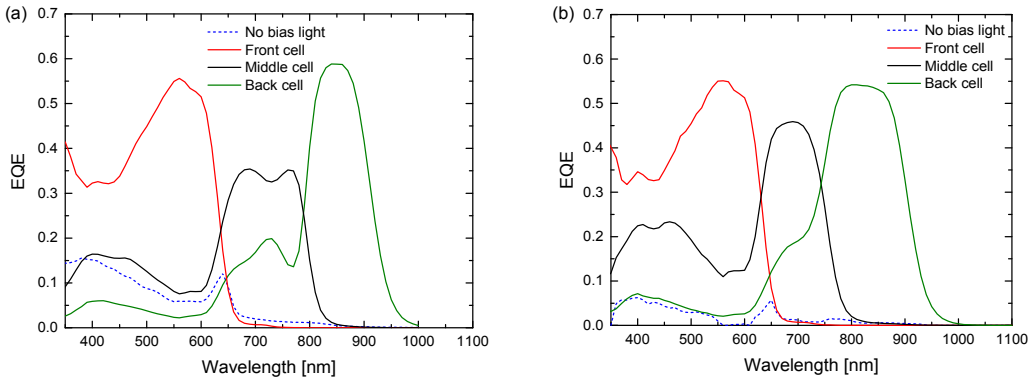

Figure 8. (a) EQE measurements of the best BHJ3-BHJ4-BHJ8 triple-junction device. Conditions for light and voltage bias: Front cell: 730 nm LED at 87 mW cm^{-2} and V_{bias} = 1.29 V; Middle cell: 530 nm LED at 44 mW cm^{-2} with 940 nm LED at 78 mW cm^{-2} and V_{bias} =1.36 V; (signal was scaled by the light-intensity-dependence factor 0.95); Back cell: 530 nm LED at 67 mW cm^{-2} and V_{bias} = 1.45 V. (b) EQE of the best BHJ3-BHJ5-BHJ8 triple-junction device. Conditions for illumination bias and voltage bias can be found in Ref. [59]

To improve the performance of the triple junction cell, we used PTB7-Th instead of PDPPTPT as the absorber layer for the middle cell. PTB7-Th:$PC_{70}BM$ (BHJ5) has opto-electronic properties close to PDPPTPT:$PC_{60}BM$ (BHJ4) but has a significantly higher IQE of 0.82 (at 145 nm), opening up the possibility of a higher current in a triple-junction solar cell. We optimized the triple device with BHJ3, BHJ5, and BHJ8 as front, middle, and back subcells using the semi-empirical method described above.[59] The optimal thicknesses found were 130, 140, and 90 nm for the front, middle, and back subcells, respectively. For this combination, a PCE of 10% was predicted and the corresponding experimental results are reported in Table 4. The EQE in Figure 8b reveals that the BHJ5 middle cell provides a significantly enhanced performance compared to BHJ4 as middle cell (Figure 8a). Because of the small blue-shift in the absorption of BHJ5 compared to BHJ4, also the back cell received more light, increasing the width of its peak in the EQE spectrum. Consequently, the EQE-integrated J_{SC} values for the front, middle and back subcells were, respectively: 7.16, 6.61, and 7.53 mA cm^{-2}. In addition to this, a remarkable FF of 0.68 was determined for such a complex stack of 8 layers sequentially processed by spin-coating and 2 additional layers by thermal evaporation.

2.7. Synopsis

By considering the results for the tandem and triple junction cells, we find that the combination of D-PEDOT:PSS/nanoparticle ZnO allowed us to use the same coating techniques to make a wide variety of layer stacks with different active layers in multi-junction devices. Besides its versatility for processing, the D-PEDOT:PSS/nanoparticle ZnO ICL matches the energy levels of the active layers adopted with very few exceptions where the V_{OC} dropped by more than 50 mV (partially due to contact issues of one of the chosen materials, PDCBT). Regarding the FF, only a small loss was observed for some of the tandems compared to the individual subcell devices. Using opto-electrical optimization and by fabricating triple-junction cells, we demonstrated that the D-PEDOT:PSS/nanoparticle ZnO combination provides an almost loss-less ICL. State-of-the-art triple-junction polymer solar cell with 10% power conversion efficiency were fabricated in excellent yields (15/16) where the PCE is limited by the photoactive layers.

3. Conclusions

We developed novel ink formulations to deposit virtually loss-less interconnecting layers for solution processed *n-i-p* multi-junction polymer solar cells, using PEDOT:PSS, ZnO or PEIE. By selecting suitable co-solvents, we improved the film-forming properties of the dispersions and solutions from which these materials were processed, while preserving their optical, electrical and structural properties. The formulations are relatively simple and can be used with a wide range of active layer materials of different chemical nature without adjustments.

For tandem cells both ZnO and PEIE are convenient as ETL of an ICL. We reported the results of six different tandem cells with nearly loss-less ICL performance. For fabricating triple-junction solar cells we find that PEIE is not suitable in the bottom ICL because it deteriorates upon deposition of the top ICL. We hypothesize that the very thin layer of PEIE (< 10 nm) in the bottom ICL might intermix with the PEDOT:PSS at their interface as a consequence of the processing of another layer of PEDOT:PSS on top of the middle cell. This problem is avoided by using ZnO nanoparticles. By a more judicious choice of the active layer materials and opto-electrical optimization, the efficiency of the triple-junction cells was improved to 10%, with very good reproducibility, demonstrating that the ICL allows to achieve state-of-the-art performance.

The new formulations of PEDOT:PSS, diluted in a near azeotropic water/*n*-propanol mixture, and ZnO nanoparticles, dispersed in isoamyl alcohol, represent a versatile combination to fabricate a nearly loss-less ICL for solution-processed multi-junction *n-i-p* polymer solar cells. It alleviates the tedious task of developing and adjusting the ICL for each specific case. We encourage researchers to adopt these layers for optimizing future multi-junction devices with novel and improved active layer materials.

4. Experimental

Materials: Pre-patterned ITO (150 nm) on glass substrates were purchased from Naranjo Substrates. Molybdenum trioxide powder (99.97%) was purchased from Sigma Aldrich. The ZnO was either made by a sol-gel route or from pre-formed nanoparticles with average diameter of 4 nm, as confirmed by dynamic light scattering measurements (see the Supporting Information for the synthesis). The sol-gel consisted of a solution 0.5 M $Zn(CH_3COO)_2 \cdot 2H_2O$ (98 %, Acros Organics) and 0.5 M ethanolamine in 2-methoxyethanol. The suspension of D-PEDOT:PSS was prepared starting from the commercial formulation Clevios P VPAl 4083. After filtering it with a PVDF 0.45 μm filter we diluted it with *n*-propanol while vigorously stirring. For the optimal dilution ratio of 1:2 we added *n*-propanol (1 mL) to VPAl 4083 (0.5 mL) in 15 minutes. The suspension was prepared fresh every time, right before depositing PEDOT:PSS, and no further additives were used. PEIE was purchased from Sigma Aldrich (batch 04814BGV). Starting from the pristine concentration in water, which was 37 wt.%, we diluted in isopropanol until the total mass fraction of PEIE became 0.2 wt.% (tandems BHJ1-BHJ6, BHJ2-BHJ4 and BHJ7-BHJ7) or 0.1 wt.% (single-junction cell of BHJ1 in Table 2 and tandem BHJ4-BHJ6). No particular stirring or additional operation were used after the addition and the solution was stable for more than 3 weeks. $PC_{60}BM$ and $PC_{70}BM$ were purchased from Solenne B.V.

PCDTBT was purchased from 1-Material (batch YY7276) and blended with $PC_{70}BM$ in a 1:4 (w/w) ratio in chlorobenzene at a polymer concentration of 7 mg mL^{-1}. PBDTTPD[60] was mixed with $PC_{70}BM$ in a 1:1.5 (w/w) ratio in chlorobenzene with 5 vol.% of 1-chloronaphthalene at a polymer concentration of 8 mg mL^{-1}. PDCBT[41] was blended with $PC_{60}BM$ in a 1:1 (w/w) ratio in chloroform containing 1 vol.% of *o*-dichlorobenzene at a polymer concentration of 10 mg mL^{-1}. PDPP5T[42] was combined with $PC_{60}BM$ in 1:2 (w/w) ratio in chloroform with 10 vol.% *o*-dichlorobenzene at a polymer concentration of 6 mg mL^{-1}. PDPP3T[61] was blended with $PC_{60}BM$ 1:2 (w/w) and dissolved in chloroform with 7 vol.% *o*-

dichlorobenzene at a polymer concentration of 5 mg mL^{-1}. The methylated derivative PMDPP3T[13] was blended with $PC_{60}BM$ 1:3 (w/w) and dissolved in chloroform containing 7 vol.% *o*-dichlorobenzene at a polymer concentration of 4 mg mL^{-1}. PDPPTPT[61] was blended with $PC_{60}BM$ 1:2 (w/w) or $PC_{70}BM$ 1:2 (w/w) in chloroform with 6 vol.% *o*-dichlorobenzene at a polymer concentration of 5 mg mL^{-1}. PTB7-Th was purchased from 1-Material, mixed with $PC_{70}BM$ (1:1.5 w/w) and dissolved in chlorobenzene containing 3 vol.% diiodooctane at a concentration of 9 mg mL^{-1}(reference and tandem cells) or 12 mg mL^{-1} (triple junction cells) of polymer.[45]

Device fabrication: Pre-patterned ITO-coated glass substrates were cleaned by sonication in acetone, followed by water and sodium dodecyl sulfate in water. After rinsing in water they were again sonicated in isopropanol. To finish the cleaning, 30 min of UV-ozone treatment preceded the spin-coating of the first layer. Sol-gel ZnO was cast directly on clean ITO substrates by spin-coating in ambient air and annealed at 150 °C for 5 min on a hotplate. The D-PEDOT:PSS dispersion was processed by spin-coating (45 nm for BHJ1-BHJ6 and 60 nm for BHJ2-BHJ4 and BHJ4-BHJ6 with PEIE) or dynamic spin-coating (45 nm for BHJ1-BHJ4, BHJ7-BHJ7, BHJ3-BHJ5, BHJ5-BHJ8 tandems and the BHJ3-BHJ5-BHJ8 triple, and 30 nm for all the other tandems and triples) in a nitrogen filled glove box for improved wetting. The layer was kept in the vacuum at ~10^{-2} mbar for 30 min right after spin-coating to remove residual solvents and no further treatment was performed. The PEIE solution was cast by spin-coating in air to form a very thin (~10 nm) layer. The ZnO nanoparticle dispersion was dynamically spin-coated in ambient air to give a 20 nm thick layer, without any post treatment. The last step in the fabrication of each of these devices was the evaporation of the top contact. In all cases this was accomplished by evaporating MoO_x (10 nm), followed by Ag (100 nm) in a vacuum chamber at ca. 6×10^{-7} mbar, through a shadow mask. On each substrate, the intersection of the ITO pattern with the evaporated top contact formed two squares of 9 mm^2 area and two squares of 16 mm^2 area. The thickness of each layer was measured using a Veeco Dektak profilometer.

Single-junction cells: Cleaned ITO substrates were covered with 40 nm of sol-gel ZnO. Subsequently, the active layer was spin-coated following different procedures. BHJ1 (85 nm) was spin-coated in a glove box and annealed at 70 °C for 10 min. BHJ2 (50 nm) was also spin-coated in a glove box and used without thermal annealing. BHJ3 (130 nm) was deposited in a glove box and annealed at 100 °C for 5 min and again at 105 °C for 5 min after evaporation of the top contact to improve the V_{OC}. Spin-coating of BHJ4 (85 nm) was performed in air. BHJ5

(85 nm) was cast in a glove box and the samples were kept at ~10^{-2} mbar for 2 h after spin-coating. BHJ6 (100 nm), BHJ7 (130 nm) and BHJ8 (110 nm) were spin-coated in air without any post-treatment. After depositing the active layer, all cells were completed by evaporating the top contact.

For the BHJ1 devices reported in Table 2, PEIE was deposited on ITO, followed by the BHJ1 layer as reported. D-PEDOT:PSS was deposited by spin-coating in a nitrogen filled glovebox from 1:1, 1:2, 1:3, 1:4 and 1:5 (v/v) dispersions in water/*n*-propanol. The top contact in this case was Ag (100 nm).

For the single-junction cells shown in Figure 4, D-PEDOT:PSS was deposited by spin-coating on clean ITO substrates to form a 45 nm thick layer and the samples were dried at ~10^{-2} mbar for 30 min. PEIE was spin-coated from solutions with different solid content (0.1, 0.2 and 0.4 wt.%). BHJ7 (130 nm) was then spin-coated in air without any post treatment. The top contact was thermally evaporated.

For the solar cells of BHJ4 shown in Figure 6, D-PEDOT:PSS was spin-coated in a glove box directly on clean ITO substrates to form a 45 nm thick layer. The samples were kept in vacuum at ~10^{-2} mbar for 30 min. PEIE or ZnO nanoparticles were then spin-coated, followed by the active layer of BHJ4 (85 nm). The water/*n*-propanol (1:2 v/v) mixture or another layer of D-PEDOT:PSS was spin-coated on top of the active layer, followed by the evaporation of the top contact.

Tandem cells: Cleaned ITO substrates were covered with 40 nm sol-gel ZnO. The active layer of the front cell was processed as described for the single-junctions cells, except for the tandem BHJ4-BHJ8 (Table 3), where the BHJ4 layer was 145 nm thick. Then D-PEDOT:PSS was processed as described before. For the BHJ3-BHJ4 and BHJ3-BHJ5 tandem cells a second annealing step of the front cell was performed at 105 °C for 5 min to improve the V_{OC}. To complete the ICL, either PEIE or the ZnO nanoparticles were deposited as reported. Deposition of the back cells followed the same procedure as for the single cells, except for the BHJ3-BHJ4 tandem (Table 3), where the back cell of BHJ4 was 145 nm thick. The top contact was formed by evaporation.

The tandem BHJ1-BHJ4 differed from the others by an additional layer of D-PEDOT:PSS (30 nm) between the BHJ4 back cell and the top contact. Also the tandem BHJ5-BHJ8 differed from the others, using another layer of D-PEDOT:PSS between ITO and the first layer of ZnO nanoparticles.

Triple-junction devices: For all the triple-junction cells, the fabrication started from sol-gel ZnO (40 nm) on clean ITO substrates, followed by the first active layer as described above. Subsequently D-PEDOT:PSS was deposited with a thickness of 30 nm (BHJ1-BHJ4-BHJ6 and BHJ3-BHJ4-BHJ8) or 45 nm (BHJ3-BHJ5-BHJ8). Whenever the front cell was BHJ3, a post annealing at 105 °C for 5 min was performed. After this, ZnO nanoparticles were deposited. For the middle cell, the same thickness of BHJ4 as for the single cells was used in the first, non-optimal triple of Table 4. As a consequence of the optimization, a thicker active layer was used in the second triple, in order to absorb more light: 145 nm. Also for the last triple a thicker active layer of BHJ5 was adopted: 140 nm. On top of the middle cell, another layer of D-PEDOT:PSS was processed in the same way as in the bottom ICL of each triple. Then ZnO nanoparticles followed to complete the second ICL. After this, the top cell was spin-coated as described for single-junction cells, with the only difference that the thickness of BHJ8 in the last triple was 90 nm. To finish, the top contact was evaporated.

Characterization: All measurements were performed under N_2 atmosphere. In order to photo-dope the ZnO and MoO_x layers, 6 min of UV exposition were performed right before the measurement for all cells. The characteristic *J-V* curve was measured from −2 V to +2 V for single and double-junction cells and to +2.6 V for triples. The number of voltage steps was 401, with an integration time of 20 ms at each point. Simulated solar light from a tungsten-halogen lamp filtered with a UV filter and daylight filter (Hoya LB120) was shined on the cells during the measurement of the *J-V* characteristics. The color of the spectrum and the intensity of it were adjusted to match the EQE-integrated J_{SC} of the single-junction cells, to warrant that the PCE can be determined from the *J-V* characteristics. To accurately define the active area of the cells, the 4 squares from the intersection of top and bottom contact were masked with an aperture slightly smaller than their size: 6.76 and 12.96 mm^2 for the 9 and 16 mm^2 squares, respectively.

The EQE was measured using a custom-made setup consisting of the following: a tungsten-halogen lamp, a chopper, a monochromator (Oriel, Cornerstone 130), a pre-amplifier (Stanford Research Systems SR570) and a lock-in amplifier (Stanford Research Systems SR830 DSP). Although the setup was in ambient air, the substrates were constantly kept sealed in a N_2 filled box equipped with a quartz window. For this measurement, a circular aperture size of 2 mm of diameter was used to define the active area. To convert the current signal from the cell into an EQE value, a comparison was made with a reference calibrated silicon solar cell. In the range of wavelengths 350-1050 nm, the standard deviation of this setup is less than

0.005 electrons/photons. As bias light, a 530, 730, and 940 nm high power LEDs from Thorlabs were involved.

Optical modeling: This was done using the transfer matrix (TM) method using Setfos 3.2 software (Fluxim AG). By measuring transmission and reflection of each layer, we estimated the *n* and *k* values as a function of the wavelength. To optimize the thickness of each active layer in the triples, we used an extension of a procedure already published for tandems.[57] This consisted in modeling iteratively the current generation of each subcell, correcting it for the corresponding IQE. The combination of this data with the normalized *J-V* characteristics of the subcells returned the *J-V* characteristics of the triple for each of the tested combination of thicknesses. The determination of the voltage bias correction for the EQE of the two optimized triples followed the reported procedure.[59]

Acknowledgements

We thank Dr. Harm van Eersel for developing scripts to calculate the optical parameters and optimize the triple-junction. This project has received funding from the European Community's Seventh Framework Programme (FP7/2007-2013) under the Grant Agreement no. 607585 project OSNIRO. The research leading to these results has also received funding from the European Research Council under the European Union's Seventh Framework Programme (FP/2007-2013) / ERC Grant Agreement No. 339031. The research forms part of the Solliance OPV program and has received funding from the Ministry of Education, Culture and Science (Gravity program 024.001.035).

References

[1] G. Li, R. Zhu, Y. Yang, *Nat. Photon.* **2012**, *6*, 153.

[2] R. Søndergaard, M, Hösel, D. Angmo, T. T. Larsen-Olsen, F. Krebs, *Mater. Today* **2012**, *15*, 36.

[3] F. Liu, Y. Gu, J. W. Jung, W. H. Jo, T. P. Russell, *J. Polym. Sci. B: Polym. Phys.* **2012**, *50*, 1018.

[4] K.-S. Chen, J.-F. Salinas, H.-L. Yip, L. Huo, J. Hou, A. K.-Y. Jen, *Energy Environ. Sci.* **2012**, *5*, 9551.

[5] C.-C. Chen, L. Dou, J. Gao, W. H. Chang, G. Li, Y. Yang, *Energy Environ. Sci.* **2013**, *6*, 2714.

[6] G. Xu, L. Shen, C. Cui, S. Wen, R. Xue, W. Chen, H. Chen, J. Zhang, H. Li, Y. Li, Y. Li, *Adv. Funct. Mater.* **2017**, *27*, 1605908.

[7] M. Kaltenbrunner, M. S. White, E. D. Glowacki, T. Sekitani, T. Someya, N. S. Sariciftci, S. Bauer, *Nat. Commun.* **2012**, *3*, 1772.

[8] R. Ma, J. Feng, D. Yin, H.-B. Sun, *Org. Electron.* **2017**, *43*, 77.

[9] W. Zhao, S. Li, H. Yao, S. Zhang, Y. Zhang, B. Yang, J. Hou, *J. Am. Chem. Soc.* **2017**, *139*, 7148.

[10] Y. Cui, H. Yao, B. Gao, Y. Qin, S. Zhang, B. Yang, C. He, B. Xu, J. Hou, *J. Am. Chem. Soc.* **2017**, *139*, 7302.

[11] J. Y. Kim, K. Lee, N. E. Coates, D. Moses, T.-Q. Nguyen, M. Dante, A. J. Heeger, *Science* **2007**, *317*, 222.

[12] L. Dou, J. You, J. Yang, C.-C. Chen, Y. He, S. Murase, T. Moriarty, K. Emery, G. Li, Y. Yang, *Nat. Photonics* **2012**, *6*, 180.

[13] W. Li, A. Furlan, K. H. Hendriks, M. M. Wienk, R. A. J. Janssen, *J. Am. Chem. Soc.* **2013**, *135*, 5529.

[14] S. Sista, M.-H. Park, Z. Hong, Y. Wu, J. Hou, W. L. Kwan, G. Li, Y. Yang, *Adv. Mater.* **2010**, *22*, 380.

[15] J. Yang, J. You, C.-C. Chen, W.-C. Hsu, H. Tan, X. W. Zhang, Z. Hong, Y. Yang, *ACS Nano* **2011**, *5*, 6210.

[16] H. Zhou, Y. Zhang, C. K. Mai, S. D. Collins, G. C. Bazan, T. Q. Nguyen, A. J. Heeger, *Adv. Mater.* **2015**, *27*, 1767.

[17] K. Zhang, K. Gao, R. Xia, Z. Wu, C. Sun, J. Cao, L. Qian, W. Li, S. Liu, F. Huang, X. Peng, L. Ding, H.-L. Yip, Y. Cao, *Adv. Mater.* **2016**, *28*, 4817.

[18] Z. Zheng, S. Zhang, J. Zhang, Y. Qin, W. Li, R. Yu, Z. Wei, J. Hou, *Adv. Mater.* **2016**, *28*, 5133.

[19] Y. Gao, V. M. Le Corre, A. Gaïtis, M. Neophytou, M. A. Hamid, K. Takanabe, P. M. Beaujuge, *Adv. Mater.* **2016**, *28*, 3366.

[20] Y. Ma, S.-C. Chen, Z. Wang, W. Ma, J. Wang, Z. Yin, C. Tang, D. Cai, Q. Zheng, *Nano Energy* **2017**, *33*, 313.

[21] S. Esiner, H. Van Eersel, M. M. Wienk, R. A. J. Janssen, *Adv. Mater.* **2013**, *25*, 2932.

[22] T. Becker, S. Trost, A. Behrendt, I. Shutsko, A. Polywka, P. Görrn, P. Reckers, C. Das, T. Mayer, D. Di Carlo Rasi, K. H. Hendriks, M. M. Wienk, R. A. J. Janssen, T. Riedl, *Adv. Energy Mater.* **2017**, DOI: 10.1002/aenm.201702533.

[23] A. R. b. M. Yusoff, H. P. Kim, J. Jang, *Energy Technol.* **2013**, 1, 212.

[24] X. Du, O. Lytken, M. S. Killian, J. Cao, T. Stubhan, M. Turbiez, P. Schmuki, H.-P. Steinrück, L. Ding, R. H. Fink, N. Li, C. J. Brabec, *Adv. Energy Mater.* **2017**, 7, 1601959.

[25] X. Guo, F. Liu, W. Yue, Z. Xie, Y. Geng, L. Wang, *Org. Electron.* **2009**, *10*, 1174.

[26] S. Sista, Z. Hong, M.-H. Park, Z. Xu, Y. Yang, *Adv. Mater.* **2010**, *22*, E77.

[27] C.-C. Chen, W.-H. Chang, K. Yoshimura, K. Ohya, J. You, J. Gao, Z. Hong, Y. Yang, *Adv. Mater.* **2014**, *26*, 5670.

[28] V. C. Tung, J. Kim, L. J. Cote, J. Huang, *J. Am. Chem. Soc.* **2011**, *133*, 9262.

[29] J. Gilot, M. M. Wienk, R. A. J. Janssen, *Appl. Phys. Lett.* **2007**, *90*, 143512.

[30] A. R. B. M. Yusoff, S. J. Lee, J. Kim, F. K. Shneider, W. J. da Silva, J. Jang, *ACS Appl. Mater. Interfaces* **2014**, *6*, 13079.

[31] S. K. Hau, H.-L. Yip, K.-S. Chen, J. Zou, A. K.-Y. Jen, *Appl. Phys. Lett.*, 2010, **97**, 253307.

[32] Z. Zheng, S. Zhang, M. Zhang, K. Zhao, L. Ye, Y. Chen, B. Yang, J. Hou, *Adv. Mater.* **2015**, *27*, 1189.

[33] Y. Zhou, C. Fuentes-Hernandez, J. W. Shim, T. M. Khan, B. Kippelen, *Energy Environ. Sci*. **2012**, *5*, 9827

[34] J. Lee, H. Kang, J. Kong, K. Lee, *Adv. Energy Mater.* **2014**, *4*, 1301226.

[35] J. Yang, R. Zhu, Z. Hong, Y. He, A. Kumar, Y. Li, Y. Yang, *Adv. Mater.* **2011**, *23*, 3465.

[36] J. C. Gustafsson, B. Liedberg, O. Inganäs, *Solid State lonics* **1994**, *69*, 145.

[37] S. Esiner, G. W. P. van Pruissen, M. M. Wienk, R. A. J. Janssen, *J. Mater. Chem. A*, **2016**, *4*, 5107.

[38] C. Tao, S. Ruan, X. Zhang, G. Xie, L. Shen, X. Kong, W. Dong, C. Liu, W. Chen, *Appl. Phys. Lett.* **2008**, *93*, 193307.

[39] N. Blouin, A. Michaud, M. Leclerc, *Adv. Mater.* **2007**, *19*, 2295.

[40] C. Dyer-Smith, I. A. Howard, C. Cabanetos, A. El Labban, P. M. Beaujuge, F. Laquai, *Adv. Energy Mater.* **2015**, *5*, 1401778.

[41] M. Zhang, X. Guo, W. Ma, H. Ade, J. Hou, *Adv. Mater.* **2014**, *26*, 5880.

[42] M. Dueggeli, M. Zaher Eteish, P. Hayoz, O. F. Aebischer, M. Fonrodona Turon, M. G. R. Turbiez, *PCT Int Appl.* **2010**, WO 2010049323

[43] J. C. Bijleveld, A. P. Zoombelt, S. G. J. Mathijssen, M. M. Wienk, M. Turbiez, D. M. de Leeuw, R. A. J. Janssen, *J. Am. Chem. Soc.* **2009**, *131*, 16616.

[44] J. C. Bijleveld, V. S. Gevaerts, D. Di Nuzzo, M. Turbiez, S. G. J. Mathijssen, D. M. de Leeuw, M. M. Wienk, R. A. J. Janssen, *Adv. Mater.* **2010**, *22*, E242.

[45] S. H. Liao, H. J. Jhuo, Y. S. Cheng, S. A. Chen, *Adv. Mater.* **2013**, *25*, 4766.

[46] S. Kouijzer, S. Esiner, C. H. Frijters, M. Turbiez, M. M. Wienk, R. A. J. Janssen, *Adv. Energy Mater*. **2012**, *2*, 945.

[47] J. Jo, J.-R. Pouliot, D. Wynands, S. D. Collins, J. Y. Kim, T. L. Nguyen, H. Y. Woo, Y. Sun, M. Leclerc, A. J. Heeger, *Adv. Mater.* **2013**, *25*, 4783.

[48] J.-H. Kim, C. E. Song, H. U. Kim, A. C. Grimsdale, S.-J. Moon, W. S. Shin, S. K. Choi, D.-H. Hwang, *Chem. Mater.* **2013**, *25*, 2722

[49] P.-N. Yeh, T.-H. Jen, Y.-S. Cheng, S.-A. Chen, *Sol. Energy Mater. Sol. Cells* **2014**, *120*, 728.

[50] J.-H. Kim, C. E. Song, B. S. Kim, I.-N. Kang, W. S. Shin, D.-H Hwang, *Chem. Mater.* **2014**, *26*, 1234.

[51] C.-Y. Chang, L. Zuo, H.-L. Yip, C.-Z. Li, Y. Li, C.-S. Hsu, Y.-J. Cheng, H. Chen, A. K.-Y. Jen, *Adv. Energy Mater.* **2014**, *4*, 1301645.

[52] D. Gupta, M. M. Wienk, R. A. J. Janssen, *ACS Appl. Mater. Interfaces* **2014**, *6*, 13937.

[53] S. Lu, H. Lin, S. Q. Zhang, J. H. Hou, W. C. H. Choy, *Adv. Energy Mater*. **2017**, DOI: 10.1002/aenm.201701164.

[54] S. M. Rowan, M. I. Newton, F. W. Driewer, G. McHale, *J. Phys. Chem. B* **2000**, *104*, 8217.

[55] Y. Zhou, C. Fuentes-Hernandez, J. Shim, J. Meyer, A. J. Giordano, H. Li, P. Winget, T. Papadopoulos, H. Cheun, J. Kim, M. Fenoll, A. Dindar, W. Haske, E. Najafabadi, T. M. Khan, H. Sojoudi, S. Barlow, S. Graham, J.-L. Brédas, S. R. Marder, A. Kahn, B. Kippelen, *Science* **2012**, *336*, 327.

[56] D. Bahro, M. Koppitz, A. Mertens, K. Glaser, J. Mescher, A. Colsmann, *Adv. Energy Mater.* **2015**, *5*, 1501019.

[57] J. Gilot, M. M. Wienk, R. A. J. Janssen, *Adv. Mater.* **2010**, *22*, 67.

[58] A. Hadipour, B. de Boer, P. W. M. Blom, *Org. Electron*. **2008**, *9*, 617.

[59] D. Di Carlo Rasi, K. H. Hendriks, M. M. Wienk, R. A. J. Janssen, *Adv. Energy Mater.* **2017**, *7*, 1701664.

[60] G. Pirotte, J. Kesters, P. Verstappen, S. Govaerts, J. Manca, L. Lutsen, D. Vanderzande, W. Maes, *ChemSusChem* **2015**, *8*, 3228.

[61] K. H. Hendriks, G. H. L. Heintges, V. S. Gevaerts, M. M. Wienk, R. A. J. Janssen, *Angew. Chemie Int. Ed.* **2013**, *52*, 8341.

Novel formulations of PEDOT:PSS in water/*n*-propanol and ZnO nanoparticles in isoamyl alcohol enable fabricating a lossless charge recombination layer for efficient inverted tandem and triple-junction solar cells for a range of polymer-fullerene photoactive layers without adjusting the deposition conditions.

Keywords: organic multi-junction solar cells, charge recombination layer, interconnection layer, inverted organic solar cells

*Dario Di Carlo Rasi, Koen H. Hendriks, Gaël H. L. Heintges, Giulio Simone, Gerwin H. Gelinck, Veronique S. Gevaerts, Ronn Andriessen, Geert Pirotte, Wouter Maes, Weiwei Li, Martijn M. Wienk, and René A. J. Janssen**

A universal route to fabricate *n-i-p* multi-junction polymer solar cells via solution processing